KIDS MAKING NOISE:
Presenting Noise Spectra of Aluminum MKIDs for Astronomy

[a]NASA Goddard Space Flight Center
[b]The University of Maryland, College Park

Carolyn Volpert,[a,b] Emily Barrentine,[a] Alberto Bolatto,[a] Ari Brown,[a] Larry Hess,[a] Thomas Stevenson,[a] Eric Switzer [a]

Abstract

Since the field has identified microwave kinetic inductance detectors (MKIDs) as a competitive candidate for future applications in infrared and sub-millimeter wave detection, it is increasingly important to establish the materials and techniques that produce highly sensitive, well-understood, and consistent detectors. We present new noise power spectral density (PSD) measurements for several thin film (25nm) aluminum coplanar waveguide (CPW) microwave resonators. We include noise PSD measurements for several bath temperatures and photon occupation numbers. We examine the trends exhibited by the fractional frequency noise spectra of our detectors at 1 kHz as a function of bath temperature and power. For our lowest temperature data (58mK) and a readout power of -84 dBm we observe fractional frequency noise in the range $S_{\delta f} / f_r^2$ = a few x10^{-17}. We observe a roughly $S_{\delta f} / f_r^2$ (1 kHz) $\propto P_{int}^{-0.5}$ relationship between internal power and fractional frequency noise at 1 kHz. We attempted more complex fits to the PSDs, but concluded that more measurements are needed to converge on meaningful fits to the data.

Introduction: The Resonators

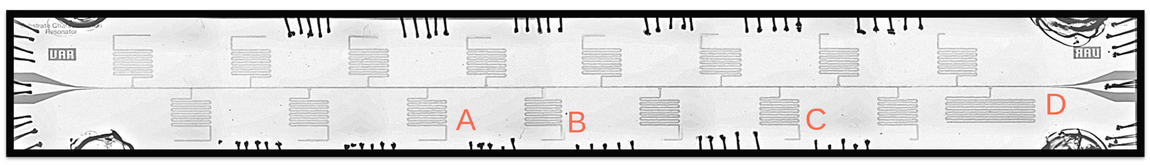

Figure 1: Image of the measured device containing 16 CPW resonators coupled to a CPW feedline (wirebonded into a package). The resonators are etched into a 25nm Al layer sputter deposited onto a Si wafer [1]. Counting from the left, resonators A, B, C, and D correspond to resonators 6, 8, 12, and 16. Resonator D is a half-wave resonator, the rest are quarter-wave resonators. The feedline was designed with an impedance of 50 Ohms, in the case of an ideal perfect conductor. This CPW device template was designed to be used to measure several materials, and is optimized for rapid turnaround of devices since it requires the patterning of only a single layer. For this reason the device incorporates a variety of coupling capacitor designs to provide wide coverage for different internal quality factors. The coupling capacitor structure lengths and corresponding design Q_c's for each resonator are shown in Table 1.

Resonator	Measured f_r (GHz)	Measured Q_i^{-1} (x10^5)	Measured Q_c^{-1} (x10^5)	Tuning Length (μm)	Coupling Finger Length (μm)
A	3.614	1.3	4.4	276	0
B	3.653	0.4	1.4	204	10
C	3.708	1.4	3.3	96	0
D*	3.910	0.6	0.7	300	30

***Note:** Resonator D is a half-wave resonator (all others are quarter-wave).

Table 1: The parameters of the resonators displayed in this work. Due to time and readout constraints, we selected four resonators from this device for extensive measurement. Accompanying each resonator, 'off resonance' data was taken for the feedline outside of the resonator band to remove system noise effects. Tuning length and coupling finger length are parameters from the device design. The measured values are from fits to data at T_{bath} = 58 mK and P_{input} = -84 dBm.

PSD Fitting Equations

$$S_{xx} = \frac{A}{1+(2\pi f\tau)^2} + Bf^{-n} + C \quad (1)$$

$$S_{xx} = \left(\frac{\alpha_k \gamma S_2}{4N_0\Delta_0}\right)^2 \frac{4n_{qp}\tau_{qp}}{V}\left(1+\frac{\tau_{qp}}{\tau_{\max}}\right) + S_{xx,0} \quad (2)$$

[3]

1 kHz Noise Trends

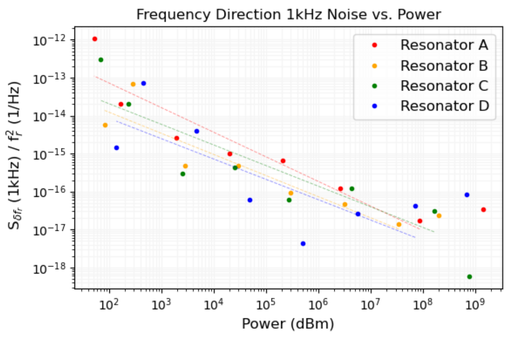

Figure 4: The frequency direction $S_{\delta f} / f_r^2$ at 1 kHz for a range powers, with power at the input of the device converted into photons generated within the resonator (as a function of Q_{total}, Q_c and f_r). The different colors denote different resonators. Linear fits to the log data vs. the internal power generated in the resonator indicate a power-law relation of $S_{\delta f} / f_r^2 \propto P^{-0.5}$ with some small variance for A through D respectively (the highest power induced bifurcation, and was excluded from fitting). For a resonator PSD that is TLS dominated, we expect $S_{\delta f} / f_r^2 \propto P_{int}^{-1/2}$, indicating. This small difference in exponents is likely due to our imperfect removal of system noise, meaning there is some small residual component of the resonator PSDs that cannot be ascribed to TLS.

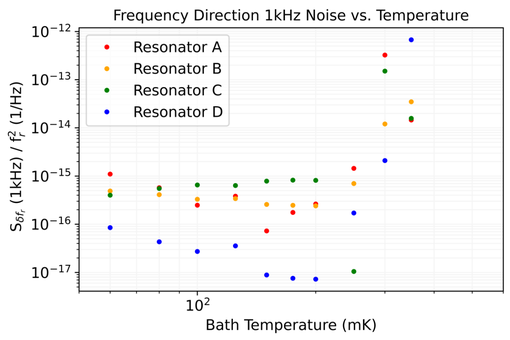

Figure 5: The frequency direction $S_{\delta f} / f_r^2$ at 1 kHz for a range temperatures with fixed power (P_{input} = -114 dBm). The different colors denote different resonators. As bath temperature increases above a certain threshold, enough quasiparticles are thermally generated to allow contributions from generation-recombination noise to dominate over TLS contributions. In future next steps include fitting this data to the model in Eq. 2.

Conclusions and Future Work

A preliminary examination of a series of noise power spectral densities taken for our resonators at several read powers indicates a relationship of $S_{\delta f} / f_r^2$ (1 kHz) $\propto P^{-0.5}$. Examining the profile of our $S_{\delta f} / f_r^2$ vs. power PSDs, we see evidence of two level system effects dominating low frequency noise contributions at low and intermediate powers. A preliminary examination of our PSDs at different temperatures suggests that we begin to see generation recombination noise dominate over TLS contributions at T_{bath} > 200 mK (> 0.15 T_c). We made a first attempt at fitting our data to Eq. 1 and Eq. 2, but found that we need more measurements to reduce statistical uncertainty in the PSDs before we are able to converge on our fits. Our next steps include repeating several of our measurements, and fitting the data to extract resonator characteristics.

Carrie Volpert
PhD Candidate
University of Maryland

References

[1] Volpert, Carolyn, et al, "Low Loss Thin Film Al-on-Si Microwave Resonators for Astronomy Applications" *19th Conference on Low Detector Physics* (2021)
[2] Noroozian, Omid. Superconducting microwave resonator arrays for submillimeter/far-infrared imaging. California Institute of Technology, 2012.
[3] McGeehan, R., et al. "Low-temperature noise performance of SuperSpec and other developments on the path to deployment." *Journal of Low Temperature Physics* 193 (2018): 1024-1032.

Noise vs. Tone Power Data

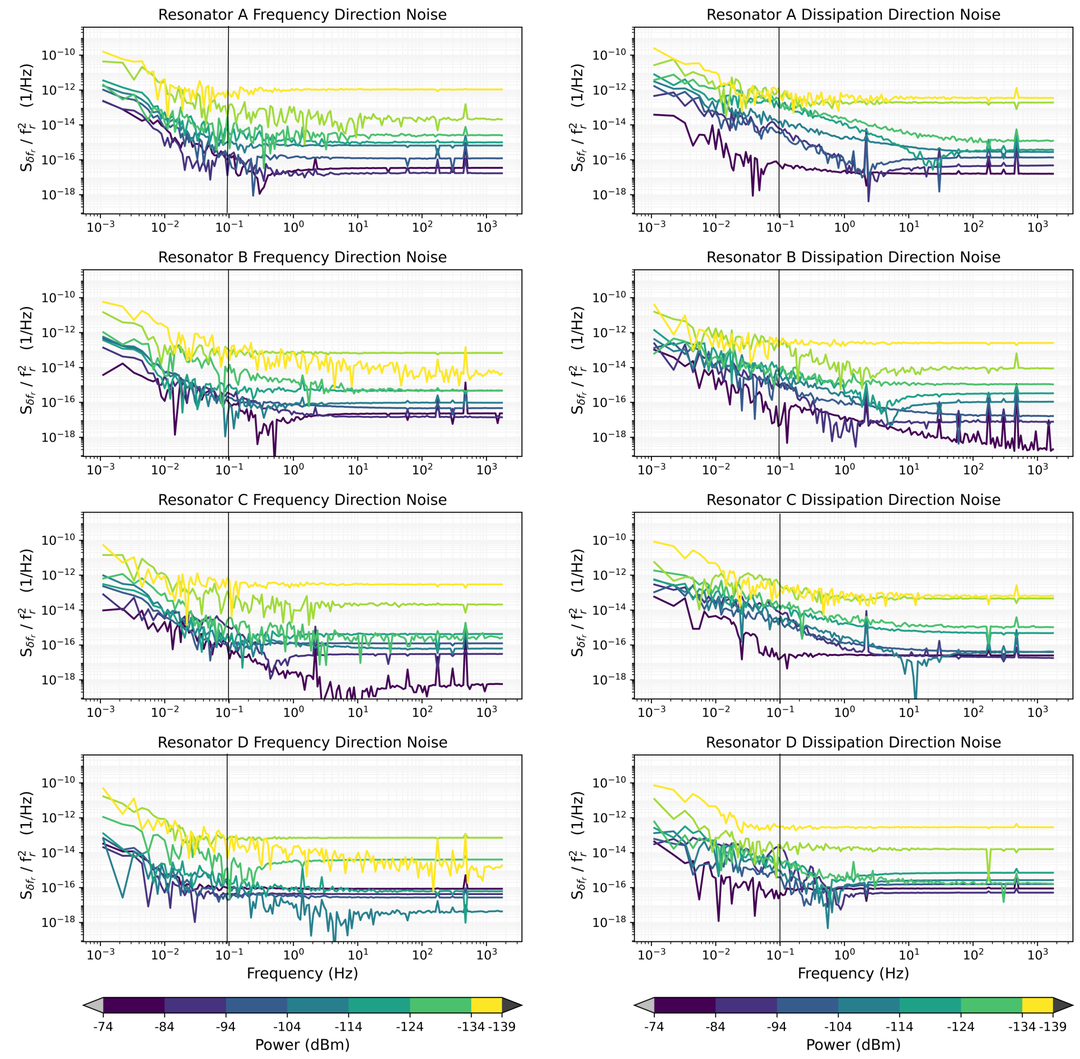

Figure 2: The y-axes correspond to: **Left** – The power spectral densities (PSDs) of the fractional frequency noise with respect to the resonant frequency (in units of 1/Hz) [2]; Relates to the noise at the resonant frequency caused by frequency shifting effects in resonator. **Right** – The power spectral densities (PSDs) of the dissipation frequency noise with respect to the resonant frequency Relates to the noise at the resonant frequency caused by power dissipating effects in the resonator. The x-axes are the frequency axis of the PSDs.

Each figure in the column depicts a series of noise spectra taken for each resonator at several powers (holding a fixed temperature, T_{bath} = 58 mK). The color bar indicates the powers entering the device at the cold stage (after attenuation) in dBm. The powers have an error of +/- 2 dBm. We have made an attempt to remove system noise (including amplifier noise) from the PSDs, and have re-binned the data to improve statistical uncertainty. The lowest frequencies in the PSDs correspond to noise originating from the cryogenic system (left of black line), frequencies above around x10^{-1} are more indicative of behavior in the resonators (right of black line). An attempt was made to fit this data to a model (Eq. 1), but more measurements are still needed for the model to converge on a fit to the data.

At the lowest read powers the PSDs are effectively flat at frequencies corresponding to resonator noise, as poor signal to noise in the device leads white noise to dominate the PSD. At intermediate powers, we begin to see a 1 / f^n component from two-level-system (TLS) noise dominate at low frequencies corresponding to the resonator, with white noise continuing to dominate at high frequencies. At the very highest powers, as the generation-recombination noise from readout power excitations becomes sufficient to saturate TLS, we just begin to see some effects of generation-recombination noise in the resonator.

Noise vs. Temperature Data

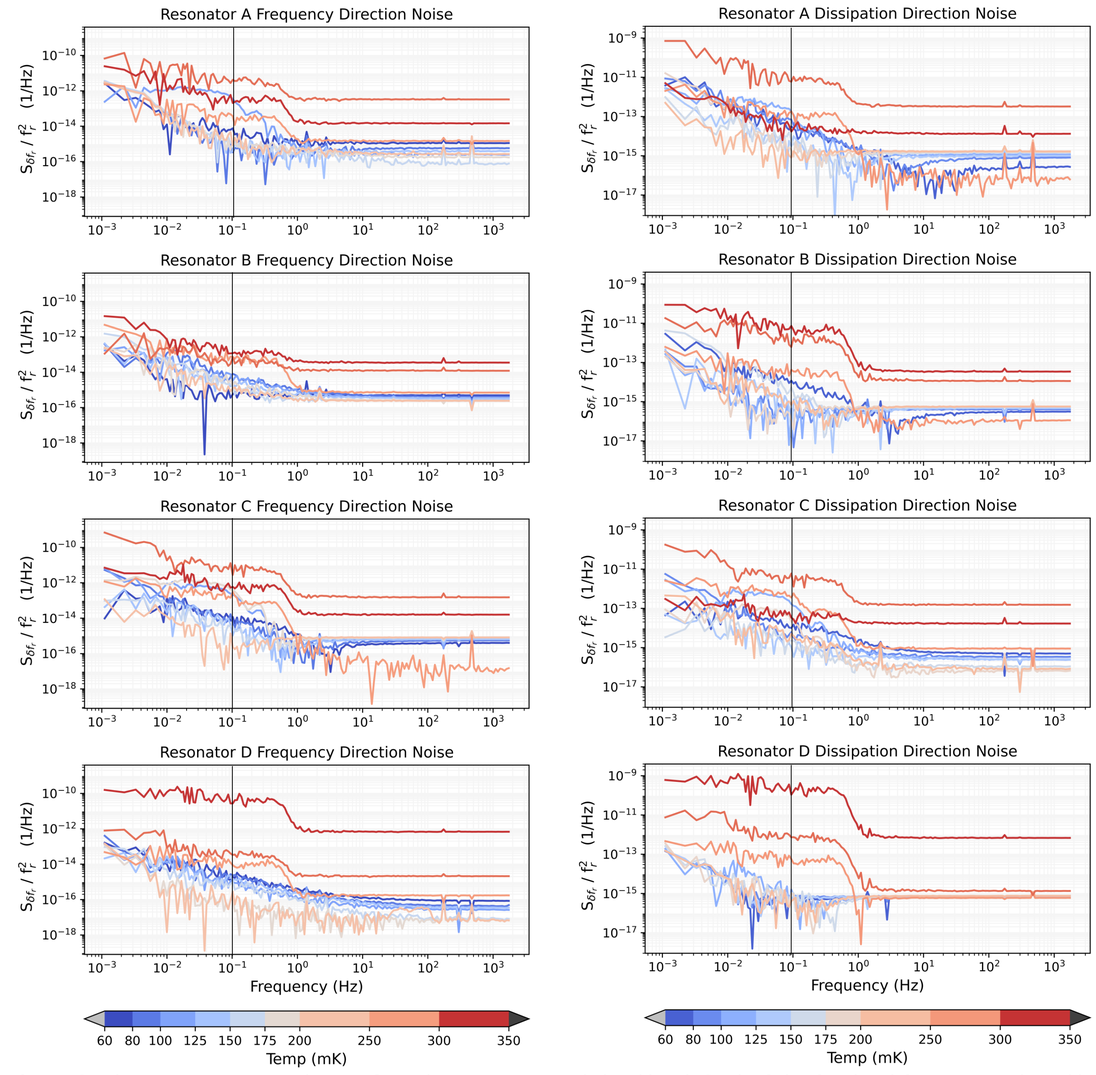

Figure 3: The y-axes correspond to: **Left** – The power spectral densities (PSDs) of the fractional frequency noise with respect to the resonant frequency (in unite of 1/Hz); Relates to the noise at the resonant frequency caused by frequency shifting effects in resonator. **Right** – The power spectral densities (PSDs) of the dissipation frequency noise with respect to the resonant frequency; Relates to the noise at the resonant frequency caused by power dissipating effects in the resonator. The x-axes are the frequency axis of the PSDs. The lowest frequencies in the PSDs correspond to noise originating from the cryogenic system (left of black line), frequencies above around x10^{-1} are more indicative of behavior in the resonators (right of black line). An attempt was made to fit this data to a model (Eq. 1), but more measurements are still needed for the model to converge on a fit to the data.

Each figure in the column depicts a series of noise spectra taken for each resonator at many temperatures (with a fixed power, P_{input} = -114 +/- 2 dBm). The color bar indicates the bath temperatures (in mK) at the stage where the device is mounted. We have made an attempt to remove system noise (including amplifier noise) from the PSDs, and have re-binned the data to improve statistical uncertainty.

At the highest bath temperatures (T_{bath}>200) we see a distinctive rolloff contribution from generation-recombination noise dominating at low frequencies corresponding to the resonator, as thermal energy from the bath begins to generate quasiparticles in the resonators and this generation-recombination contribution dominates over saturated TLS. At lower temperatures, the 1 / f^{-n} contribution is seen to dominate over generation-recombination noise.